

Supplementary Materials for

Mismatch-repair deficiency predicts response of solid tumors to PD-1 blockade

Dung T. Le, Jennifer N. Durham, Kellie N. Smith, Hao Wang, Bjarne R. Bartlett, Laveet K. Aulakh, Steve Lu, Holly Kemberling, Cara Wilt, Brandon S. Luber, Fay Wong, Nilofer S. Azad, Agnieszka A. Rucki, Dan Laheru, Ross Donehower, Atif Zaheer, George A. Fisher, Todd S. Crocenzi, James J. Lee, Tim F. Greten, Austin G. Duffy, Kristen K. Ciombor, Aleksandra D. Eyring, Bao H. Lam, Andrew Joe, S. Peter Kang, Matthias Holdhoff, Ludmila Danilova, Leslie Cope, Christian Meyer, Shibin Zhou, Richard M. Goldberg, Deborah K. Armstrong, Katherine M. Bever, Amanda N. Fader, Janis Taube, Franck Housseau, David Spetzler, Nianqing Xiao, Drew M. Pardoll, Nickolas Papadopoulos, Kenneth W. Kinzler, James R. Eshleman, Bert Vogelstein, Robert A. Anders, Luis A. Diaz Jr.*

*Corresponding author. Email: ldiaz@mskcc.org

Published 8 June 2017 on *Science* First Release
DOI: 10.1126/science.aan6733

This PDF file includes:

Materials and Methods

Figs. S1 to S4

Tables S1 to S7

References

Other supplementary material for this manuscript includes:

Tables S8 to S10 (Excel format)

SUPPLEMENTARY METHODS

PATIENTS

To be eligible for participation in this study, patients had to be at least 18 years of age, have histologically confirmed evidence of previously-treated, progressive carcinoma. All patients underwent MMR status testing prior to enrollment. All patients had at least one measurable lesion as defined by the Response Evaluation Criteria in Solid Tumors (RECIST), version 1.1, an Eastern Cooperative Oncology Group (ECOG) performance-status score of 0 or 1, and adequate hematologic, hepatic, and renal function. Eligible patients with CRC must have received at least 2 prior cancer therapies and patients with other cancer types must have received at least 1 prior cancer therapy. Patients with untreated brain metastases, history of HIV, hepatitis B, hepatitis C, clinically significant ascites/effusions, or autoimmune disease were excluded.

A total of 86 patients with treatment-refractory progressive, metastatic, mismatch repair-deficient cancers were recruited from six centers for this phase II trial. Additional longitudinal data from eleven colorectal cancer and seven non-colorectal cancer patients mismatch repair-deficient cancers from our previous study were included (19). For study enrollment, mismatch repair-deficiency was determined at each participating institution by immunohistochemistry for mismatch repair proteins or by PCR-based tests for microsatellite instability. Confirmation of mismatch-repair deficiency in each patient enrolled in the study was performed at a central location. When sufficient tissue was available, microsatellite instability in DNA purified from the tumor was assessed with an MSI Analysis System (Promega).

STUDY OVERSIGHT

Initial drafts of the manuscript were prepared by a subset of the authors and all authors contributed to the final manuscript. All the authors made the decision to submit the manuscript for publication. The Principal Investigator (D. Le) and the Investigational New Drug Sponsor (L. Diaz) vouch for the accuracy and completeness of the data reported as well as adherence to the protocol.

The protocol was approved by the institutional review board at each site. All patients provided written informed consent before study entry. The Principal Investigator and the Investigational New Drug Sponsor were responsible for oversight of the study. Merck & Co., Inc., Kenilworth, NJ USA donated the study drug and reviewed the final drafts of the protocol and of this manuscript before submission; they did not participate in the analysis of the data.

MISMATCH REPAIR STATUS TESTING (27, 28)

Six slides of tumor and normal (uninvolved lymph node or margin of resection) were cut (5 microns each), deparaffinized (xylene), and one stained with hematoxylin and eosin (H+E). A tumor area containing at least 20% neoplastic cells, designated by a board-certified Anatomic Pathologist was macrodissected using the Pinpoint DNA isolation system (Zymo Research, Irvine, CA), digested in proteinase K for 8 hours and DNA was isolated using a QIAamp DNA Mini Kit (Qiagen, Valencia, CA). MSI was assessed using the MSI Analysis System (Promega, Madison, WI), composed of 5 pseudomonomorphic mononucleotide repeats (BAT-25, BAT-26, NR-21, NR-24 and MONO-27) to detect MSI and 2-pentanucleotide repeat loci (PentaC and PentaD) to confirm identity between normal and tumor samples, per manufacturer's instructions.

Following amplification of 50-100 ng DNA, the fluorescent PCR products were sized on an Applied Biosystems 3130xl capillary electrophoresis instrument (Invitrogen, Calsbad, CA). Pentanucleotide loci confirmed identity in all cases. Controls included water as a negative control and a mixture of 80% germline DNA with 20% MSI cancer DNA as a positive control. The size in bases was determined for each microsatellite locus and tumors were designated as MSI if two or more mononucleotide loci varied in length compared to the germline DNA.

STUDY DESIGN

Original Version 1/May 1, 2013 through Amendment 6/Version 7/November 19, 2014 (Reported Le et al., N Engl J Med 2015; 372:2509-2520)

This phase II trial was initially conducted and reported (19) using a parallel two-stage design to simultaneously evaluate the efficacy of MK-3475 and MSI as a treatment selection marker for anti-PD-1 therapy. It consisted of two-stage phase 2 studies in parallel in the three cohorts of patients: patients with MSI positive colorectal adenocarcinomas (Cohort A); patients with MSI negative colorectal adenocarcinomas (Cohort B); and patients with MSI positive solid tumor malignancies but not colorectal adenocarcinoma (Cohort C). The study agent, pembrolizumab, was administered at 10 mg/kg intravenously every 14 days. Pembrolizumab is a humanized monoclonal anti-PD-1 antibody of the IgG4 kappa isotype that blocks the interaction between PD-1 and its ligands, PD-L1 and PD-L2. Safety assessments were performed before each treatment. Radiographic assessments were performed at week 12, then every 8 weeks during the first year and every 12 weeks thereafter. Post-treatment biopsies were obtained from measurable lesions after 4 or 20 weeks.

After the endpoint was met successfully (19), the trial was expanded to enroll additional patients in Cohorts A and C (allowing up to a total of 75 subjects in Cohort A and up to 71 subjects in Cohort C) to estimate the efficacy of pembrolizumab in patients with mismatch repair-deficient cancers. The sample size represented the feasible number of MSI patients the study can enroll in two years. For each of Cohort A and B, the co-primary endpoints were progression-free-survival (irPFS) at 20 weeks and objective response (irOR) assessed using immune related criteria. A step-down gatekeeping procedure was used to preserve the overall type I error. A two-stage Green-Dahlberg design was used to evaluate irPFS, with interim and final analysis after 15 and 25 patients, respectively. At stage 1, ≥ 1 of 15 free-of-progression at 20 weeks were required to proceed to the second stage, and ≥ 4 of 25 free-of-progression at 20 weeks were then required to proceed to test for irOR, with ≥ 4 of 25 responders (irCR or irPR) indicating promising efficacy in that cohort. Each cohort could be terminated for efficacy as soon as ≥ 4 free-of-progression at 20 weeks and ≥ 4 responses were confirmed, or be terminated for futility as soon as 0 of 15 in stage 1 were free-of-progression at 20 weeks or ≥ 22 subjects had disease progression by 20 weeks. This design achieves 90% power to detect a 20-week irPFS rate of 25% and 80% power to detect an irOR rate (irORR) of 21%, with an overall type I error of 0.05 at the null hypothesis of 20-week irPFS rate of 5% and irORR of 5%.

For Cohort C, the primary endpoint was irPFS at 20 weeks. A two-stage Green-Dahlberg two-stage design was used, with an interim and final analysis after 14 and 21 patients; at stage 1, ≥ 1 of 14 free-of-progression at 20 weeks were required to proceed to the second stage, with ≥ 4 of 21 free-of-progression at 20 weeks at the end indicating adequate efficacy in Cohort C. The cohort could be terminated as soon as ≥ 4 free-of-progression at 20 weeks were confirmed. The design has 81% power to detect a 20-week irPFS rate of 25% with a 5% type I error at the null hypothesis of 20-week irPFS rate of 5%.

Amendment 7/Version 8/May 1, 2015 Changes

Since the emerging clinical data suggest promising clinical activity, up to an additional 50 patients could be enrolled into Cohorts A and C (Up to a total of 75 in Cohort A and 71 in Cohort C). Tumor assessments with this addition of the expansion will be evaluated by RECIST 1.1 criteria only. This amendment enables eligible patients to gain access to the promising new treatment of MK-3475. The increased number of patients allows response rate and other efficacy endpoints to be estimated with greater precision. The sample size represents the feasible number of MSI patients the study can enroll in two years.

STATISTICAL ANALYSIS

Original Version 1/May 1, 2013 through Amendment 6/Version7/November 19, 2014 (Reported Le et al., N Engl J Med 2015; 372:2509-2520)

Response and progression were evaluated using RECIST v1.1 and the immune-related response criteria (irRC) adopted from Wolchok et al. (29), which uses the sum of the products of bidimensional tumor measurements and incorporates new lesions into the sum. Progression-free survival (PFS) rates and irPFS rate at 20-weeks was estimated as the proportion of patients who were free-of-disease progression and alive at 20 weeks after the initiation of pembrolizumab. Patients who had disease progression prior to 20 weeks or were enrolled for >20 weeks at the time the study data were collated were included in the analysis for estimating 20-week PFS (irPFS) rate. Patients who dropped out early due to toxicities or worsening disease and therefore did not have 20-week tumor assessment were considered as having progressive disease. ORR (irORR) was the proportion of patients who achieved best overall response of CR or PR (irCR or irPR). Patients who were in the study long enough to have tumor response evaluations were included in the analysis for estimating response rates. Among those who responded (CR or PR), duration of response was the time of first RECIST response to the time of disease progression, and was censored at the last evaluable tumor assessment for responders who had not progressed.

PFS and irPFS were defined as the time from the date of initial dose to the date of disease progression or the date of death due to any cause, whichever occurred first. PFS and irPFS were censored on the date of the last evaluable tumor assessment documenting absence of progressive disease for patients who were alive and progression-free. Overall survival (OS) was defined as the time from the date of initial dose to death due to any cause. For patients who were still alive at the time of analysis, the OS time was censored on the last date the patients were known to be alive. Survival times were summarized by the Kaplan-Meier method. As a *post hoc* analysis, log-rank tests were used to compare Cohort A and B and hazard ratios were estimated based on Cox models.

The association of percent CEA decline after 1 cycle with PFS or OS was assessed using landmark analysis based on Cox regression models. For correlative studies, non-parametric Wilcoxon test was used to compare mutational load between MMR-deficient and MMR-proficient patients. The effects of baseline mutational burden and immune markers on response and survival times were examined using logistic regression and Cox regression, respectively.

The primary objective of this study was to estimate the efficacy of pembrolizumab in patients with mismatch repair-deficient cancers. The primary end points for Cohorts A and C were the best overall objective response based on Response Evaluation Criteria in Solid Tumors (RECIST) 1.1. Objective response rates were estimated as the proportion of patients who achieved a complete response (CR) or partial response (PR), along with exact binomial 95%

confidence intervals. Progression-free survival and overall survival rates were calculated as the means in the Kaplan–Meier method.

IMMUNOHISTOCHEMISTRY & IMAGE ANALYSIS

The fraction of malignant cells exhibiting a membranous pattern of B7-H1 expression and the percentage at the invasive front were quantified by three pathologists (R.A.A., F.B., and J.M.T.) as previously reported (30, 31). Image analysis was used to determine the number of CD8 diaminobenzidine (DAB)-stained cells. Using the H&E-stained slide for each case, we identified the following regions: i) tumor, ii) invasive front (the boundary between malignant and non-malignant tissue), and iii) normal tissue. The CD8-stained slides were scanned at 20x equivalent magnification (0.49 micrometers per pixel) on an Aperio ScanScope AT. Regions corresponding to tumor, invasive front and normal tissue (above, from the H&E) were annotated on separate layers using Aperio ImageScope v12.1.0.5029.

CD8-positive lymphocyte density was calculated in each of the above regions using a custom algorithm implemented in PIP (32). Results were converted to Deepzoom images using the VIPs library (33) and visualized using the OpenSeadragon viewer (<http://openseadragon.github.io>).

Amendment 7/Version 8/May 1, 2015 Changes through Amendment 8/Version 9/November 20, 2015

Response and progression were evaluated using RECIST v1.1. Patients who were in the study long enough to have tumor response evaluations were included in the analysis for estimating response rates. The analysis was primarily descriptive, and was performed for each cohort separately, as well as Cohort A and Cohort C combined.

The percentages of patients who achieve CR, PR, and SD were estimated with corresponding 95% confidence interval. Best overall objective response rate (CR or PR) was reported. PFS were defined as the time from the date of initial dose to the date of disease progression or the date of death due to any cause, whichever occurred first. PFS were censored on the date of the last evaluable tumor assessment documenting absence of progressive disease for patients who were alive and progression-free. Overall survival (OS) was defined as the time from the date of initial dose to death due to any cause. For patients who were still alive at the time of analysis, the OS time was censored on the last date the patients were known to be alive. If patients were known to be alive after the data cut, the patient was censored on 12/19/16. Survival times were summarized by the Kaplan-Meier method. Response rate was also estimated by disease histology type.

IFN ELISpot ASSAY

IFN- γ production was measured by a standard overnight enzyme-linked immunosorbent spot (ELISpot) assay. Briefly, 96-well nitrocellulose plates (EMD Millipore, Billerica, MA) were coated with anti-IFN- γ monoclonal antibody (10 μ g/ml; Mabtech, Stockholm, Sweden) and incubated overnight at 4°C. Plates were washed and blocked with IMDM supplemented with 10% heat-inactivated FBS for 2 h at 37°C. T cells stimulated for 10 days with one of 8 putative MANAs were added to wells in duplicate or triplicate at 50,000 cells per well and were stimulated overnight with PBMC pre-loaded with 1 μ g/ml relevant peptide, a cytomegalovirus (CMV), Epstein-Barr virus (EBV), and influenza virus peptide pool (CEF), or no peptide in AIM V media.

T cells with PBMC alone served as negative controls. After 18h, ELISpot plates were washed and processed for spot development. Spots were counted using an automated ELISpot plate reader (AID, Strasberg, Germany). Background was calculated as the mean number of SFC/10⁶ cells in duplicate or triplicate control wells without peptide. Peptide-stimulated responses were considered positive if the mean SFC/10⁶ was significantly above this background value with an unadjusted p value <0.05.

STIMULATION AND EXPANSION OF MANA-SPECIFIC T CELLS.

T cell functional assays were performed for an MMR-deficient colorectal cancer patient with durable objective clinical response to pembrolizumab. Putative MANAs were identified by Personal Genome Diagnostics (PGDx, Baltimore, MD) using their neoantigen prediction pipeline (Supplementary Appendix). All T cells used in MANA recognition assays were derived from PBMC obtained >52 weeks after initiation of pembrolizumab treatment. Fifteen putative MANAs were synthesized (Sigma-Aldrich, St. Louis, MO) and used to stimulate T cells in vitro for 10 days followed by an IFN γ ELISpot assay (Supplementary Appendix). Seven of these MANAs were selected for further analysis based on modest IFN γ ELISpot reactivity above background (unadjusted p value <0.05). These 7 MANAs were evaluated for T cell recognition, tumor infiltration, and peripheral dynamics using a recently developed assay performed as previously described (24), with minor modifications. Briefly, on day 0 T cells were isolated from PBMC by negative selection (EasySep; STEMCELL Technologies). The T cell-negative fraction was gamma irradiated (3,000 rads) and cocultured with an equal number of negatively-selected T cells in culture media (AIM V with 50 μ g/mL gentamicin) with 1 μ g/mL relevant peptide, EBV control peptide, or no peptide and supplemented with IL-7 (25 ng/mL; Miltenyi) and IL-15 (25 ng/mL; PeproTech). IL-2 (10 IU/mL; Chiron) was added to the cultures on day 1. On day 3, half the media was replaced with fresh culture media for the same final concentrations of IL-2, IL-7, and IL-15 used previously. On day 7, half the media was replaced with fresh culture media for a final concentration of 20 IU/mL IL-2 and 25 ng/mL IL-7 and IL-15. Cells were harvested on day 10 and washed twice with PBS. Cultured T-cell pellets were flash-frozen in liquid nitrogen and stored at -140°C.

SEQUENCING ANALYSIS

Samples

Samples provided as FFPE blocks or frozen tissue underwent pathological review to determine tumor cellularity. Tumors were macrodissected to remove contaminating normal tissue, resulting in samples containing >20% neoplastic cells. Matched normal samples were provided as blood, saliva or normal tissue obtained from surgery.

Germline Analyses

DNA was isolated from frozen blood cells at Johns Hopkins and sent to Color Genomics for confirmatory testing of hereditary cancer syndromes. All patient cohorts were tested using a 30 gene panel in which germline variants lead to cancer susceptibility – this panel included the mismatch repair genes MLH1, MSH2, MSH6, and PMS2. Variants were classified as either pathogenic or of unknown significance.

Genomic Analysis

Tumor samples and matched normal peripheral-blood specimens were obtained from a subset of subjects from this study with mismatch repair-deficient carcinomas for exome sequencing. Additional details are provided in the Supplementary Appendix.

Sample Preparation and Next-Generation Sequencing (34)

Sample preparation, library construction, exome capture, next generation sequencing, and bioinformatics analyses of tumor and normal samples were performed at Personal Genome Diagnostics, Inc. (Baltimore, Maryland). In brief, DNA was extracted from frozen or formalin-fixed paraffin embedded (FFPE) tissue, along with matched blood or saliva samples using the Qiagen DNA FFPE tissue kit or Qiagen DNA blood mini kit (Qiagen, CA). Genomic DNA from tumor and normal samples were fragmented and used for Illumina TruSeq library construction (Illumina, San Diego, CA) according to the manufacturer's instructions or as previously described (35). Briefly, 50 nanograms (ng) - 3 micrograms (μg) of genomic DNA in 100 microliters (μl) of TE was fragmented in a Covaris sonicator (Covaris, Woburn, MA) to a size of 150-450bp. To remove fragments smaller than 150bp, DNA was purified using Agencourt AMPure XP beads (Beckman Coulter, IN) in a ratio of 1.0 to 0.9 of PCR product to beads twice and washed using 70% ethanol per the manufacturer's instructions. Purified, fragmented DNA was mixed with 36 μl of H₂O, 10 μl of End Repair Reaction Buffer, 5 μl of End Repair Enzyme Mix (cat# E6050, NEB, Ipswich, MA). The 100 μl end-repair mixture was incubated at 20°C for 30 min, and purified using Agencourt AMPure XP beads (Beckman Coulter, IN) in a ratio of 1.0 to 1.25 of PCR product to beads and washed using 70% ethanol per the manufacturer's instructions. To A-tail, 42 μl of end-repaired DNA was mixed with 5 μl of 10X dA Tailing Reaction Buffer and 3 μl of Klenow (exo-)(cat# E6053, NEB, Ipswich, MA). The 50 μl mixture was incubated at 37°C for 30 min and purified using Agencourt AMPure XP beads (Beckman Coulter, IN) in a ratio of 1.0 to 1.0 of PCR product to beads and washed using 70% ethanol per the manufacturer's instructions. For adaptor ligation, 25 μl of A-tailed DNA was mixed with 6.7 μl of H₂O, 3.3 μl of PE-adaptor (Illumina), 10 μl of 5X Ligation buffer and 5 μl of Quick T4 DNA ligase (cat# E6056, NEB, Ipswich, MA). The ligation mixture was incubated at 20°C for 15 min and purified using Agencourt AMPure XP beads (Beckman Coulter, IN) in a ratio of 1.0 to 0.95 and 1.0 of PCR product to beads twice and washed using 70% ethanol per the manufacturer's instructions. To obtain an amplified library, twelve PCRs of 25 μl each were set up, each including 15.5 μl of H₂O, 5 μl of 5 x Phusion HF buffer, 0.5 μl of a dNTP mix containing 10 mM

of each dNTP, 1.25 µl of DMSO, 0.25 µl of Illumina PE primer #1, 0.25 µl of Illumina PE primer #2, 0.25 µl of Hotstart Phusion polymerase, and 2 µl of the DNA. The PCR program used was: 98°C for 2 minutes; 12 cycles of 98°C for 15 seconds, 65°C for 30 seconds, 72°C for 30 seconds; and 72°C for 5 min. DNA was purified using Agencourt AMPure XP beads (Beckman Coulter, IN) in a ratio of 1.0 to 1.0 of PCR product to beads and washed using 70% ethanol per the manufacturer's instructions. Exonic or targeted regions were captured in solution using the Agilent SureSelect v.4 kit according to the manufacturer's instructions (Agilent, Santa Clara, CA). The captured library was then purified with a Qiagen MinElute column purification kit and eluted in 17 µl of 70°C EB to obtain 15 µl of captured DNA library. The captured DNA library was amplified in the following way: Eight 30µl PCR reactions each containing 19 µl of H₂O, 6 µl of 5 x Phusion HF buffer, 0.6 µl of 10 mM dNTP, 1.5 µl of DMSO, 0.30 µl of Illumina PE primer #1, 0.30µl of Illumina PE primer #2, 0.30 µl of Hotstart Phusion polymerase, and 2 µl of captured exome library were set up. The PCR program used was: 98°C for 30 seconds; 14 cycles (exome) or 16 cycles (targeted) of 98°C for 10 seconds, 65°C for 30 seconds, 72°C for 30 seconds; and 72°C for 5 min. To purify PCR products, a NucleoSpin Extract II purification kit (Macherey-Nagel, PA) was used following the manufacturer's instructions. Paired-end sequencing, resulting in 100 bases from each end of the fragments for exome libraries and 150 bases from each end of the fragment for targeted libraries, was performed using Illumina HiSeq 2000/2500 and Illumina MiSeq instrumentation (Illumina, San Diego, CA).

Primary Processing of Next-Generation Sequencing Data and Identification of Putative Somatic Mutations (34)

Somatic mutations were identified using VariantDx custom software (Personal Genome Diagnostics, Baltimore, Maryland) for identifying mutations in matched tumor and normal samples. Prior to mutation calling, primary processing of sequence data for both tumor and normal samples were performed using Illumina CASAVA software (v1.8), including masking of adapter sequences. Sequence reads were aligned against the human reference genome (version hg18) using ELAND with additional realignment of select regions using the Needleman-Wunsch method (36). Candidate somatic mutations, consisting of point mutations, insertions, and deletions were then identified using VariantDx across the either the whole exome or regions of interest. VariantDx examines sequence alignments of tumor samples against a matched normal while applying filters to exclude alignment and sequencing artifacts. In brief, an alignment filter was applied to exclude quality failed reads, unpaired reads, and poorly mapped reads in the tumor. A base quality filter was applied to limit inclusion of bases with reported phred quality score > 30 for the tumor and > 20 for the normal. A mutation in the tumor was identified as a candidate somatic mutation only when (i) distinct paired reads contained the mutation in the tumor; (ii) the number of distinct paired reads containing a particular mutation in the tumor was at least 10% of read pairs; (iii) the mismatched base was not present in >1% of the reads in the matched normal sample as well as not present in a custom database of common germline variants derived from dbSNP; and (iv) the position was covered in both the tumor and normal at > 150X. Mutations arising from misplaced genome alignments, including paralogous sequences, were identified and excluded by searching the reference genome.

Candidate somatic mutations were further filtered based on gene annotation to identify those occurring in protein-coding regions. Functional consequences were predicted using snpEff and a custom database of CCDS, RefSeq and Ensembl annotations using the latest transcript versions available on hg18 from UCSC (<https://genome.ucsc.edu/>). Predictions were ordered to prefer transcripts with canonical start and stop codons and CCDS or Refseq transcripts over Ensembl when available. Finally mutations were filtered to exclude intronic and silent changes, while retaining mutations resulting in missense mutations, nonsense mutations, frameshifts, or

splice site alterations. A manual visual inspection step was used to further remove artefactual changes.

Identification of putative mutation associated neoantigens (MANAs)

Detected somatic mutations, consisting of nonsynonymous single base substitutions, insertions and deletions, were evaluated for putative neoantigens using the ImmunoSelect-R pipeline (Personal Genome Diagnostics, Baltimore, MD). ImmunoSelect-R performs a comprehensive assessment of paired somatic and wild type peptides 8-11 amino acids in length at every position surrounding a somatic mutation. The protocol utilizes whole-exome-sequencing data from paired tumor/normal samples to accurately infer a patient's germline HLA allele set, which is then used to predict the MHC class I binding potential of each somatic and wild-type peptide (netMHCpan). Neoantigen candidates meeting an IC50 strength < 500nM were further characterized for putative T-cell epitope status (netCTLpan) and tumor-associated expression levels derived from TCGA to generate a final ranking of peptides for experimental follow-up.

T cell receptor (TCR) sequencing.

DNA was extracted from tumor tissue, longitudinal pre- and post-treatment PBMC, and flash-frozen peptide-stimulated T cells using the Qiagen DNA FFPE and Qiagen DNA blood mini kit, respectively (Qiagen). TCR V β CDR3 sequencing was performed using the survey (tumor and cultured cells) or deep (PBMC) resolution Immunoseq platforms (25, 26) (Adaptive Biotechnologies, Seattle, WA). Bioinformatic and biostatistical analysis of productive clones was performed to identify antigen-specific expansions using the following criteria: 1) significant expansion (Fisher exact test with Benjamini-Hochberg FDR, $p < 0.05$) compared to T cells cultured without peptide, 2) no significant expansion of the relevant clone in any other peptide-stimulated culture, including culture with a known MHC class I-restricted immunogenic EBV viral epitope, and 3) presence in the tumor. Binding and stability of MANAs that induced antigen-specific expansions were evaluated by Immunitrack (Copenhagen, Denmark) using a luminescent oxygen channeling immunoassay (LOCI) and decay measurements of the peptide:MHC class I, respectively.

Microsatellite instability testing by NGS.

Microsatellite loci in the target regions of a commercially available 592-gene NGS panel (Caris Life Sciences) were first identified with MISA (pgrc.ipk-gatersleben.de/misa/). The number of microsatellite loci altered by somatic insertions or deletions was calculated, and the count only included alterations that resulted in increases or decreases in the number of short tandem repeats. Microsatellite loci in regions that typically have lower coverage depth relative to other genomic regions were not included. Cases were considered microsatellite instable if they had 43 altered microsatellite loci, and this threshold was established by comparing to the PCR-based MSI analysis result from ~2100 cases, with a final performance of 95.8% sensitivity, 99.4% specificity, 94.5% PPV, and 99.2% NPV.

Table S1. Baseline Characteristics

Characteristic		Patients n=86
Age-years	<i>median</i>	57
	<i>range</i>	24 - 92
Sex-no. (%)	<i>Female</i>	42 (49)
	<i>Male</i>	44 (51)
ECOG performance status-no. (%)¹	0	20 (23)
	1	66 (77)
Diagnosis-no. (%)	<i>Ampulla of Vater</i>	4 (5)
	<i>Cholangiocarcinoma</i>	4 (5)
	<i>Colorectal</i>	40 (47)
	<i>Endometrial</i>	15 (17)
	<i>Gastroesophageal</i>	5 (6)
	<i>Neuroendocrine</i>	1 (1)
	<i>Osteosarcoma</i>	1 (1)
	<i>Pancreas</i>	8 (9)
	<i>Prostate</i>	1 (1)
	<i>Small Intestine</i>	5 (6)
	<i>Thyroid</i>	1 (1)
	<i>Unknown</i>	1 (1)
Histology-no. (%)	<i>well/moderately differentiated</i>	36 (42)
	<i>poorly differentiated</i>	38 (44)
	<i>other</i>	12 (14)
Stage IV-no. (%)		84 (98)
Time since first diagnosis-months*	<i>median</i>	27
	<i>range</i>	3 - 144
Prior systemic therapies-no. (%)	0	1 (1)
	1	16 (19)
	2	29 (34)
	3	23 (27)
	≥4	17 (20)
Detected germline mutation or known Lynch-no. (%)	<i>Yes</i>	39 (45)
	<i>No</i>	32 (37)
	<i>VUS</i>	3 (3)
	<i>Unknown</i>	12 (14)

¹ECOG, Eastern Cooperative Oncology Group

*Three patients excluded due to lack data

Table S2. Germline Analysis

SampleID	Cohort	Chromosome	Pos	Ref	Alt	Gene	Type	chGVS	pHGVS	Exon	Transcript	BIC	Zygoty	StructuralVariant	Classification
1	Colorectal	2	47690295	T	C	MSH2	SNV	c.1510+2T>C		9	ENST00000233146		Heterozygous		Likely Pathogenic
6	Non-Colorectal	2	47705428	C	G	MSH2	SNV	c.2228C>G	p.Ser743*	14	ENST00000233146		Heterozygous		Pathogenic
9	Colorectal	2	47629544			MSH2	SV							deletion of exons 1-6	Pathogenic
9	Colorectal	2	48033750	A	G	MSH6	SNV	c.3961A>G	p.Arg1321Gly	9	ENST00000234420		Heterozygous		Variant of Uncertain Significance
11	Colorectal	2	47641485	AC	A	MSH2	indel	c.871delC	p.Leu291*	5	ENST00000233146		Heterozygous		Pathogenic
15	Colorectal	2	47656712			MSH2	SV	c.1077-169_1661+355del						deletion of exons 7-10	Pathogenic
16	Colorectal	3	37067138	CA	C	MLH1	indel	c.1050delA	p.Gly351Aspfs*16	12	ENST00000231790		Heterozygous		Pathogenic
20	Non-Colorectal	2	47641560	A	T	MSH2	SNV	c.942+3A>T		5	ENST00000233146		Heterozygous		Pathogenic
31	Colorectal	3	37083822	G	A	MLH1	SNV	c.1731G>A	p.Ser577Ser	15	ENST00000231790		Heterozygous		Pathogenic
33	Colorectal	2	47629544			MSH2	SV							deletion of exons 1-7 (including deletion of EPCAM exons 1-9)	Pathogenic
35	Non-Colorectal	7	6029571	T	C	PMS2	SNV	c.1004A>G	p.Asn335Ser	10	ENST00000265849		Heterozygous		Variant of Uncertain Significance
36	Colorectal	3	37048493	C	A	MLH1	SNV	c.392C>A	p.Ser131*	5	ENST00000231790		Heterozygous		Pathogenic
42	Colorectal	2	47702189	CAAT	C	MSH2	indel	c.1786_1788delAAT	p.Asn596del	12	ENST00000233146		Heterozygous		Pathogenic
44	Non-Colorectal	2	48033590	G	C	MSH6	SNV	c.3802-1G>C		8	ENST00000234420		Heterozygous		Likely Pathogenic
52	Colorectal	3	37038108	A	G	MLH1	SNV	c.117-2A>G		2	ENST00000231790		Heterozygous		Pathogenic
56	Colorectal	7	6034954			PMS2	SV	c.804-?_903+?del						deletion of exon 8	Pathogenic
106	Non-Colorectal	2	47702310	G	C	MSH2	SNV	c.1906G>C	p.Ala636Pro	12	ENST00000233146		Heterozygous		Pathogenic
108	Non-Colorectal	2	47637116			MSH2	SV	c.367-?_645+?del						deletion of exon 3	Pathogenic
111	Colorectal	7	6045549	C	A	PMS2	SNV	c.137G>T	p.Ser46Ile	2	ENST00000265849		Heterozygous		Pathogenic
113	Non-Colorectal	2	47672695	C	T	MSH2	SNV	c.1285C>T	p.Gln429*	8	ENST00000233146		Heterozygous		Pathogenic
2-004	Non-Colorectal	2	47705460	A	G	MSH2	SNV	c.2260A>G	p.Thr754Ala	14	ENST00000233146		Heterozygous		Variant of Uncertain Significance
2-006	Colorectal	2	48033392	TAAAG	T	MSH6	indel	c.3699_3702delAGAA	p.Lys1233Asnfs*6	8	ENST00000234420		Heterozygous		Pathogenic
2-101	Non-Colorectal	2	48027268	ACAGT	A	MSH6	indel	c.2150_2153delTCAG	p.Val717Alafs*18	4	ENST00000234420		Heterozygous		Pathogenic
2-102	Colorectal	3	37053590	G	A	MLH1	SNV	c.677G>A	p.Arg226Gln	8	ENST00000231790		Heterozygous		Pathogenic
3-003	Colorectal	2	47641560	A	T	MSH2	SNV	c.942+3A>T		5	ENST00000233146		Heterozygous		Pathogenic
3-104	Non-Colorectal	3	37070319	A	AT	MLH1	indel	c.1456dupT	p.Ser486Phefs*17	13	ENST00000231790		Heterozygous		Pathogenic
4-003	Colorectal	3	37061871	G	T	MLH1	SNV	c.955G>T	p.Glu319*	11	ENST00000231790		Heterozygous		Pathogenic
4-005	Non-Colorectal	2	47629544			MSH2	SV							deletion of exons 1-6	Pathogenic
4-103	Colorectal	2	47629544			MSH2	SV							deletion of exons 1-6	Pathogenic
4-007	Non-Colorectal	2	47707870	G	T	MSH2	SNV	c.2494G>T	p.Glu832*	15	ENST00000233146		Heterozygous		Pathogenic
5-004	Non-Colorectal	3	37070424	G	A	MLH1	SNV	c.1558+1G>A		13	ENST00000231790		Heterozygous		Likely Pathogenic
5-101	Colorectal	7	6038803	A	C	PMS2	SNV	c.641T>G	p.Val214Gly	6	ENST00000265849		Heterozygous		Variant of Uncertain Significance
6-001	Colorectal	2	47709200			MSH2	SV	c.2635-718_*279del						deletion of exon 16	Pathogenic
6-101	Non-Colorectal	2	48030691	C	CT	MSH6	indel	c.3312dupT	p.Gly1105Trpfs*3	5	ENST00000234420		Heterozygous		Pathogenic
6-102	Non-Colorectal	3	37083822	G	A	MLH1	SNV	c.1731G>A	p.Ser577Ser	15	ENST00000231790		Heterozygous		Pathogenic
6-103	Non-Colorectal	2	48025804	G	A	MSH6	SNV	c.682G>A	p.Glu228Lys	4	ENST00000234420		Heterozygous		Variant of Uncertain Significance

Table S3. Drug-Related Adverse Events*

<i>Event-no. (%)</i>	All Grades N=84	Grade 1 or 2	Grade 3 or 4
Any	62 (74%)	62 (74%)	17 (20%)
Generalized Symptoms			
<i>Fatigue</i>	21 (25%)	19 (23%)	2 (2%)
<i>Flu-like symptoms</i>	6 (7%)	6 (7%)	0 (0%)
<i>Infection</i>	5 (6%)	5 (6%)	0 (0%)
Gastrointestinal			
<i>Diarrhea/colitis</i>	19 (23%)	14 (17%)	5 (6%)
<i>Nausea/vomiting</i>	11 (13%)	10 (12%)	1 (1%)
<i>Gastritis/ulcer</i>	4 (5%)	3 (4%)	1 (1%)
<i>Transaminitis</i>	4 (5%)	4 (5%)	0 (0%)
<i>Pancreatitis/Hyperamylasemia</i>	5 (6%)	0 (0%)	5 (6%)
Endocrine Disorders			
<i>Thyroid disease/hypophysitis</i>	18 (21%)	18 (21%)	0 (0%)
Arthritis/arthralgias	14 (17%)	12 (14%)	2 (2%)
Hematologic			
<i>Anemia</i>	6 (7%)	4 (5%)	2 (2%)
<i>Thrombocytopenia</i>	4 (5%)	3 (4%)	1 (1%)
Rash/pruritus	30 (36%)	29 (35%)	1 (1%)
Neuropathy	5 (6%)	4 (5%)	1 (1%)
Acute kidney injury	4 (5%)	3 (4%)	1 (1%)

*Included are adverse events occurring in $\geq 5\%$ of patients.

A total of 84 patients were included in the analysis with a cutoff date of 8/31/2016

Events were counted once for each patient using the highest grading

Table S4. A comparison of response to treatment between CRC and non-CRC cases

<i>Type of Response-no (%)</i>	Colorectal cancers n=40	Non-colorectal cancers n=46
<i>Complete Response</i>	5 (12)	13 (28)
<i>Partial Response</i>	16 (40)	12 (26)
<i>Stable Disease</i>	12 (30)	8 (17)
<i>Progressive Disease</i>	4 (10)	8 (17)
<i>Not Evaluable</i> ¹	3 (8)	5 (11)
<i>Objective Response Rate (%)</i>	52	54
<i>95% CI</i>	36, 68	39, 69
<i>Disease Control Rate (%)</i> ²	82	72
<i>95% CI</i>	67, 93	57, 84
<i>Median Progression-free survival (months)</i>	NR ³	18.1
<i>95% CI</i>	16.1, NR	14.3, NR
<i>2-year progression-free survival rate</i>	59	46
<i>95% CI</i>	44 - 78	30 - 72
<i>Median Overall survival (months)</i>	NR	NR
<i>95% CI</i>	NR, NR	19.3, NR
<i>2-year overall survival rate (%)</i>	72	57
<i>95% CI</i>	58 - 89	40 - 81

¹Patients were considered not evaluable if they did not undergo a 12 week scan due to clinical progression.

²The rate of disease control was defined as the percentage of patients who had a complete response, partial response or stable disease for 12 weeks or more.

³NR=Not reached

Table S5. Response to Treatment by Tumor Type

<i>Type of Response-no (%)</i>	Ampullary n=4	Cholangiocarcinoma n=4	Colorectal n=40	Endometrial n=15	Gastroesophageal n=5	Neuroendocrine n=1	Osteosarcoma n=1	Pancreas n=8	Prostate n=1	Small intestine n=5	Thyroid n=1	Unknown n=1
Complete Response	1 (25)	1 (25)	5 (12)	3 (20)	3 (60)	0 (0)	0 (0)	2 (25)	1 (100)	2 (40)	0 (0)	0 (0)
Partial Response	0 (0)	0 (0)	16 (40)	5 (33)	0 (0)	1 (100)	0 (0)	3 (37)	0 (0)	2 (40)	0 (0)	1 (100)
Stable Disease	1 (25)	3 (75)	12 (30)	3 (20)	0 (0)	0 (0)	0 (0)	1 (12)	0 (0)	0 (0)	0 (0)	0 (0)
Progressive Disease	1 (25)	0 (0)	4 (10)	3 (20)	2 (40)	0 (0)	1 (100)	0 (0)	0 (0)	1 (20)	0 (0)	0 (0)
Not Evaluable¹	1 (25)	0 (0)	3 (8)	1 (7)	0 (0)	0 (0)	0 (0)	2 (25)	0 (0)	0 (0)	1 (100)	0 (0)
Objective Response Rate (%)	25	25	52	53	60	100	0	62	100	80	N/A ³	100
Disease Control Rate (%)²	50	100	82	73	60	100	0	75	100	80	N/A	100

¹Patients were considered not evaluable if they did not undergo a 12 week scan due to clinical progression.

²The rate of disease control was defined as the percentage of patients who had a complete response, partial response or stable disease for 12 weeks or more.

Table S6. Summary post-treatment biopsies

Patient	Biopsy location	Malignant Cells	Best Response	Progression Censored	PFS (month)	OS Censor	OS (months)
6	Abdomen	Yes	PD	1	2.8	1	20.7
11	Abdomen	No	PR	0	33.5	0	35.2
15	Left Pelvis	No	CR	0	32.2	0	33.0
50	Supraclavicular lymph node	Yes	PD	1	2.9	1	9.3
51	Pelvis	No	SD	1	4.3	1	16.3
53	Pancreas	No	PR	1	18.2	0	19.8
57	Liver	No	SD	0	16.4	0	14.2
108	Liver	No	PR	0	11.8	1	7.6
112	Superclavicular lymph node	No	PD	1	3.0	1	3.0
113	Liver	Yes	PD	1	2.0	0	16.8
2-006	Liver	No	PR	0	14.8	1	11.2
2-102	Left level IV cervical lymph node	Yes	PD	1	2.7	0	9.4
2-103	Right quadrant mass	No	SD	0	8.3	0	7.0
3-102	Left supraclavicular node	No	SD	1	4.1	0	21.8
4-002	lymph node	Yes	PR	1	4.6	0	19.4
4-003	Right lower quadrant peritoneal mass	Yes	SD	0	19.4	1	19.4
4-107	Abdomen	Yes	PR	0	2.7	0	21.5
5-002	Perihepatic mass	Yes	SD	1	14.9	0	4.4
6-001	lymph node	No	SD	0	17.6	0	18.6
6-102	left cervical neck Lymph Node	No	PR	0	12.3	0	12.9

Table S7. Summary of Genomic Alterations

Pt	Tumor Type	Timing	Tissue Sequenced	Sample Type	Normal Sample	Pathological Tumor Purity	Mutation Tumor Purity	Somatic Sequence Alterations	B2M
1	Colorectal	Pre-treatment	Colorectal	FFPE	Blood	20%	59%	1,291	WT
4	Ampullary	Pre-treatment	Ampulla of Vater	FFPE	Blood	70%	85%	771	WT
6	Small bowel	Pre-treatment	Small Intestine	FFPE	Blood	10%	28%	2,138	WT
8	Colorectal	Pre-treatment	Colorectal	FFPE	Blood	20%	35%	1,681	WT
9	Colorectal	Pre-treatment	Colorectal	FFPE	Blood	10%	47%	1,814	2 frameshift deletions
11	Colorectal	Pre-treatment	Colorectal	FFPE	Blood	30%	27%	492	WT
15	Colorectal	Pre-treatment	Colorectal	FFPE	Blood	40%	47%	2,345	WT
16	Panreas	Pre-treatment	Pancreas	FFPE	Blood	50%	54%	4,025	WT
19	Colorectal	Pre-treatment	Colorectal	FFPE	Blood	40%	39%	1,477	WT
20	Ampullary	Pre-treatment	Ampulla of Vater	FFPE	Blood	N/A	56%	4,650	WT
25	Duodenal	Pre-treatment	Duodenal	FFPE	Blood	N/A	36%	1,361	V69Wfs*34
25	Duodenal	Post-treatment	Brain (Recurrence)	FFPE	Blood	60%	49%	1,407	V69Wfs*34 and 12L>P
29	Endometrial	Pre-treatment	Para-aortic Lymph node	FFPE	Blood	No_Data	47%	1,200	D96Mfs*7
30	Endometrial	Pre-treatment	Rectum	FFPE	Blood	60%	83%	2,282	101R>H
31	Colorectal	Pre-treatment	Colorectal	FFPE	Blood	30%	33%	941	WT
33	Colorectal	Pre-treatment	Colorectal	FFPE	Blood	40%	47%	1,330	WT
36	Colorectal	Pre-treatment	Colorectal	FFPE	Blood	50%	49%	1,838	T93Hfs*2 and D116lfs
42	Colorectal	Pre-treatment	Colorectal	FFPE	Blood	30-40%	25%	367	WT
44	Ampullary	Pre-treatment	Ampulla of Vater	FFPE	Blood	No_Data	38%	2,294	WT
52	Colorectal	Pre-treatment	Colorectal	FFPE	Blood	No_Data	25%	478	67+4A>G
4-002	Colorectal	Pre-treatment	Colorectal	FFPE	Blood	60%	47%	904	WT
4-002	Colorectal	Post-treatment	Brain (Recurrence)	FFPE	Blood	No_Data	46%	1,059	L15Ffs*41
6-101	Thyroid	Post-treatment	Brain	FFPE	FFPE	No_Data	81%	949	WT

Table S8. Somatic mutations in beta-2-microglobulin. See accompanying spreadsheet.

Table S9. Comparison of somatic mutations in patient 25. See accompanying spreadsheet.

Table S10. Comparison of somatic mutations in patient 4-002. See accompanying spreadsheet.

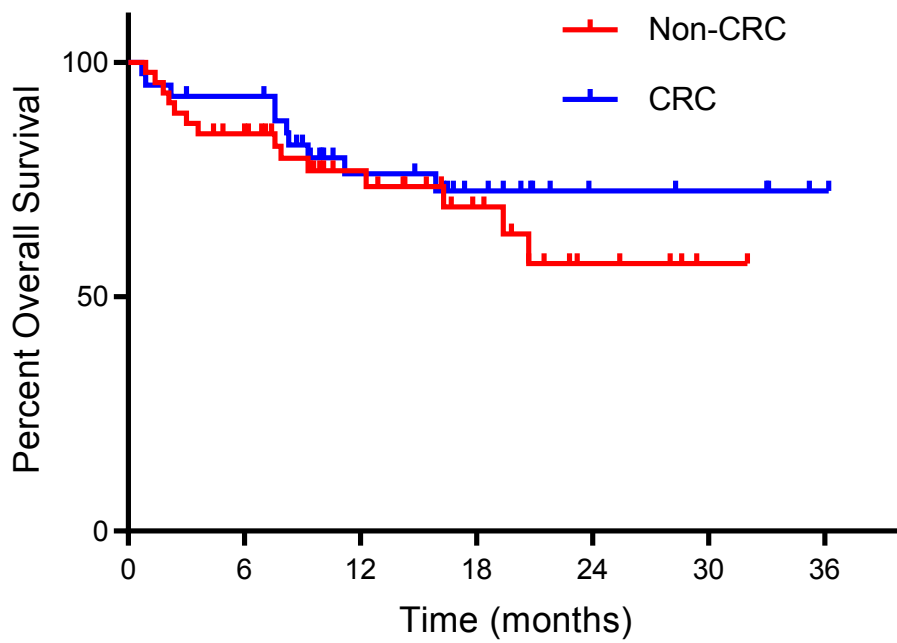
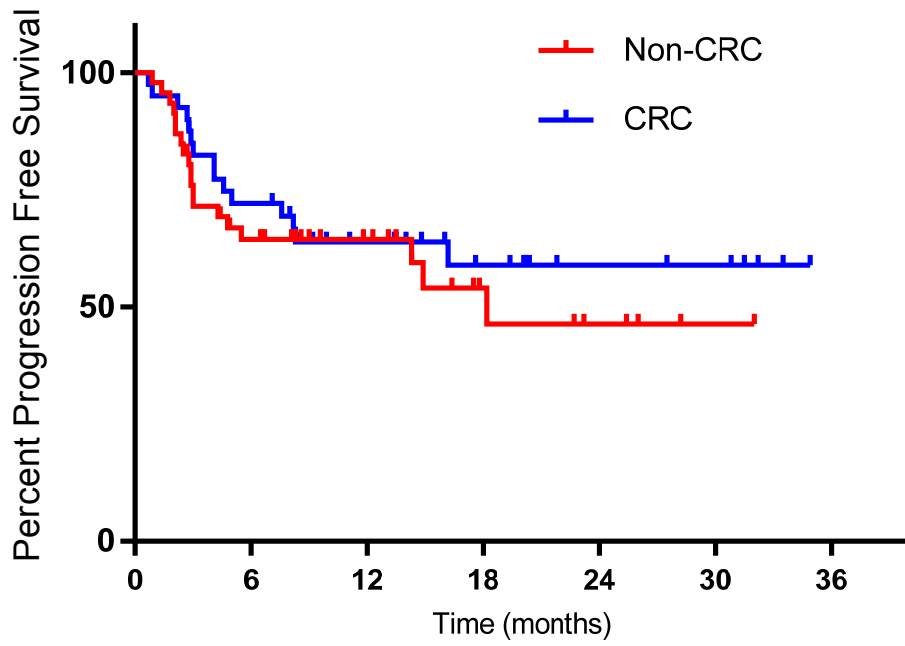


Figure S1. PFS and OS comparison between colorectal cancer (CRC) and non-CRC with mismatch repair deficiency.

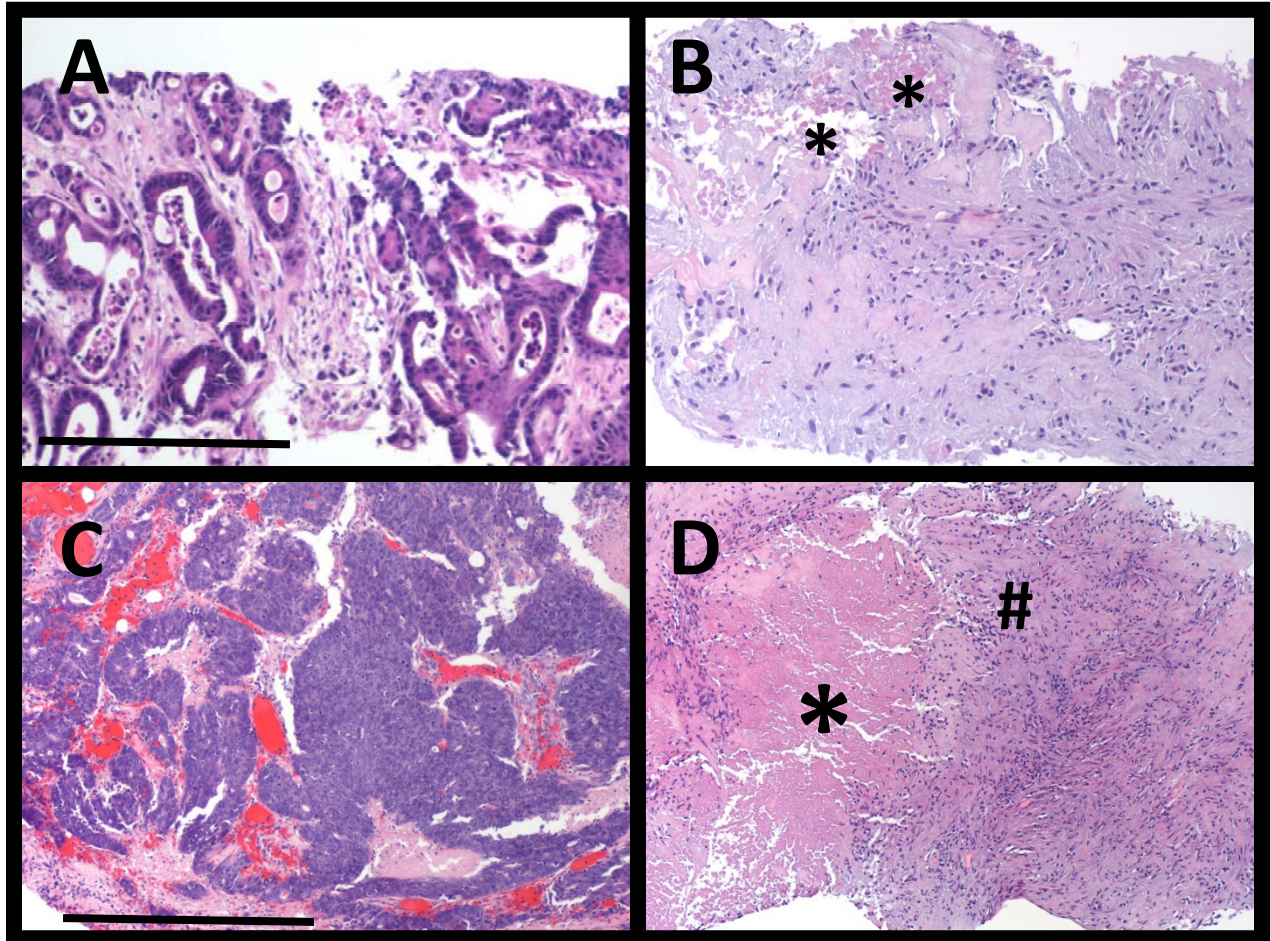


fig. S2. Histologic effects of pembrolizumab on mismatch repair deficient metastatic adenocarcinoma. (A) Pre-treatment core biopsies of metastatic colonic adenocarcinoma from Patient 15 before and (B) After therapy demonstrating focal necrosis (*), mild chronic inflammation, early hyalinizing fibrosis, and resolving granulation tissue. (Scale bar 0.25mm). (C) Pre-treatment biopsy from Patient 2-006 showing a metastatic colonic adenocarcinoma with medullary features. (D) The post-treatment biopsy shows prominent necrosis (*), loose granuloma formation (#), focal fibrosis, and moderate chronic inflammation. No malignant epithelial (neoplastic) colon cancer cells were identified. (Scale bar 0.50 mm).

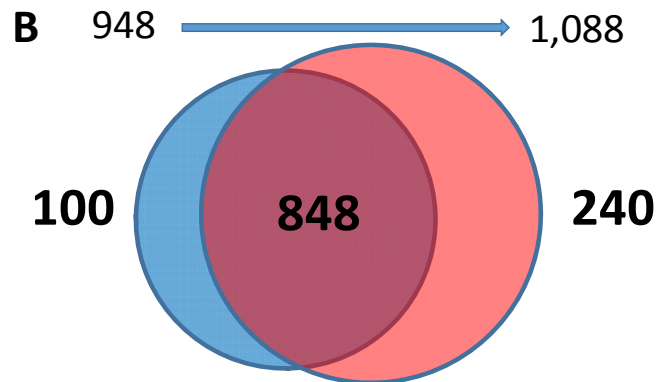
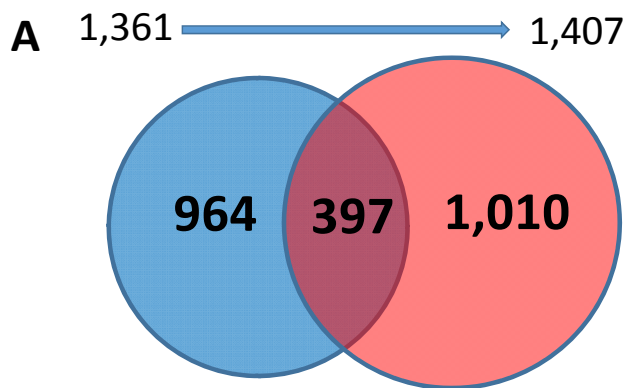
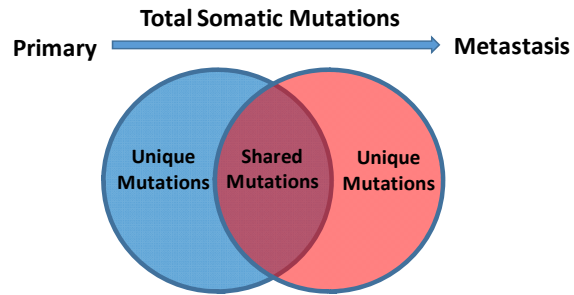


fig. S3. Total somatic mutations of acquired resistance in brain metastases of two patients. (A) Recurrence (Subject 25) showed 17% overlap of non-synonymous mutations with the primary tumor while acquiring 1,010 unique mutations. **(B)** The brain metastases (Subject 4-002) shared 71% of non-synonymous mutations with its primary and gained 240 new mutations.

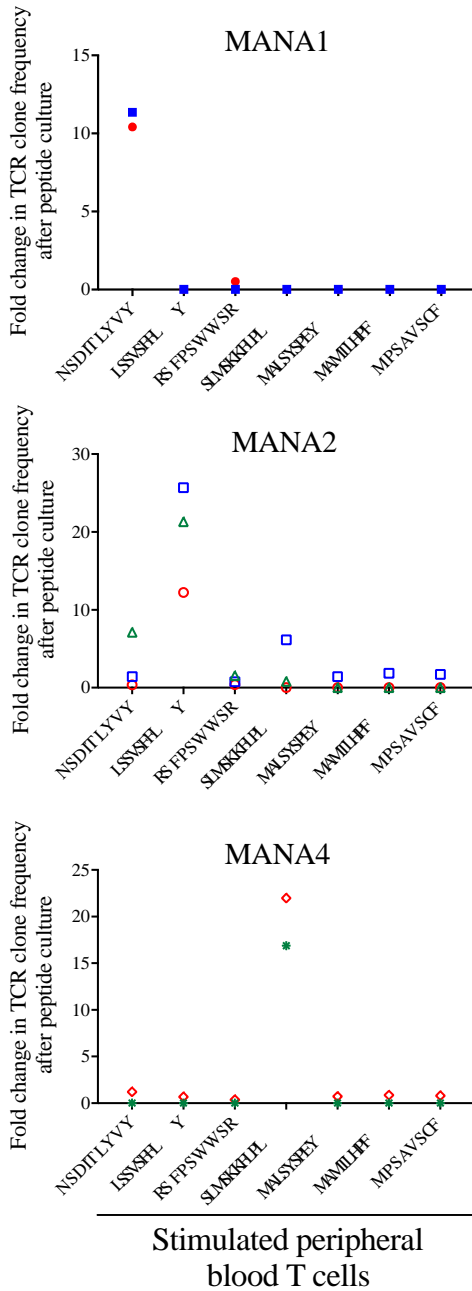


fig. S4. Specificity of MANA-specific T cell clonal expansions in a patient with durable PR to PD-1 blockade. MANA-specific T cell responses were identified against three of the seven candidate MANAs (MANA1, MANA2 and MANA4) after a 10-day in vitro stimulation (left panels) of peripheral T cells obtained from patient 19. MANA specific clones were identified by significant expansion in response to the relevant peptide and no significant expansion of that clone in response to any other peptide tested. Data are shown as the fold change in TCR clone frequency compared to the frequency of that clone after identical culture without peptide.

References

1. S. L. Topalian, C. G. Drake, D. M. Pardoll, Immune checkpoint blockade: A common denominator approach to cancer therapy. *Cancer Cell* **27**, 450–461 (2015). [doi:10.1016/j.ccell.2015.03.001](https://doi.org/10.1016/j.ccell.2015.03.001) [Medline](#)
2. P. C. Tumeh, C. L. Harview, J. H. Yearley, I. P. Shintaku, E. J. Taylor, L. Robert, B. Chmielowski, M. Spasic, G. Henry, V. Ciobanu, A. N. West, M. Carmona, C. Kivork, E. Seja, G. Cherry, A. J. Gutierrez, T. R. Grogan, C. Mateus, G. Tomasic, J. A. Glaspy, R. O. Emerson, H. Robins, R. H. Pierce, D. A. Elashoff, C. Robert, A. Ribas, PD-1 blockade induces responses by inhibiting adaptive immune resistance. *Nature* **515**, 568–571 (2014). [doi:10.1038/nature13954](https://doi.org/10.1038/nature13954) [Medline](#)
3. D. F. McDermott, C. G. Drake, M. Sznol, T. K. Choueiri, J. D. Powderly, D. C. Smith, J. R. Brahmer, R. D. Carvajal, H. J. Hammers, I. Puzanov, F. S. Hodi, H. M. Kluger, S. L. Topalian, D. M. Pardoll, J. M. Wigginton, G. D. Kollia, A. Gupta, D. McDonald, V. Sankar, J. A. Sosman, M. B. Atkins, Survival, durable response, and long-term safety in patients with previously treated advanced renal cell carcinoma receiving nivolumab. *J. Clin. Oncol.* **33**, 2013–2020 (2015). [doi:10.1200/JCO.2014.58.1041](https://doi.org/10.1200/JCO.2014.58.1041) [Medline](#)
4. S. L. Topalian, M. Sznol, D. F. McDermott, H. M. Kluger, R. D. Carvajal, W. H. Sharfman, J. R. Brahmer, D. P. Lawrence, M. B. Atkins, J. D. Powderly, P. D. Leming, E. J. Lipson, I. Puzanov, D. C. Smith, J. M. Taube, J. M. Wigginton, G. D. Kollia, A. Gupta, D. M. Pardoll, J. A. Sosman, F. S. Hodi, Survival, durable tumor remission, and long-term safety in patients with advanced melanoma receiving nivolumab. *J. Clin. Oncol.* **32**, 1020–1030 (2014). [doi:10.1200/JCO.2013.53.0105](https://doi.org/10.1200/JCO.2013.53.0105) [Medline](#)
5. S. N. Gettinger, L. Horn, L. Gandhi, D. R. Spigel, S. J. Antonia, N. A. Rizvi, J. D. Powderly, R. S. Heist, R. D. Carvajal, D. M. Jackman, L. V. Sequist, D. C. Smith, P. Leming, D. P. Carbone, M. C. Pinder-Schenck, S. L. Topalian, F. S. Hodi, J. A. Sosman, M. Sznol, D. F. McDermott, D. M. Pardoll, V. Sankar, C. M. Ahlers, M. Salvati, J. M. Wigginton, M. D. Hellmann, G. D. Kollia, A. K. Gupta, J. R. Brahmer, Overall survival and long-term safety of nivolumab (anti-programmed death 1 antibody, BMS-936558, ONO-4538) in patients with previously treated advanced non-small-cell lung cancer. *J. Clin. Oncol.* **33**, 2004–2012 (2015). [doi:10.1200/JCO.2014.58.3708](https://doi.org/10.1200/JCO.2014.58.3708) [Medline](#)
6. J. M. Taube, A. Klein, J. R. Brahmer, H. Xu, X. Pan, J. H. Kim, L. Chen, D. M. Pardoll, S. L. Topalian, R. A. Anders, Association of PD-1, PD-1 ligands, and other features of the tumor immune microenvironment with response to anti-PD-1 therapy. *Clin. Cancer Res.* **20**, 5064–5074 (2014). [doi:10.1158/1078-0432.CCR-13-3271](https://doi.org/10.1158/1078-0432.CCR-13-3271) [Medline](#)
7. N. J. Llosa, M. Cruise, A. Tam, E. C. Wicks, E. M. Hechenbleikner, J. M. Taube, R. L. Blosser, H. Fan, H. Wang, B. S. Lubner, M. Zhang, N. Papadopoulos, K. W. Kinzler, B. Vogelstein, C. L. Sears, R. A. Anders, D. M. Pardoll, F. Housseau, The vigorous immune

- microenvironment of microsatellite instable colon cancer is balanced by multiple counter-inhibitory checkpoints. *Cancer Discov.* **5**, 43–51 (2015). [doi:10.1158/2159-8290.CD-14-0863](https://doi.org/10.1158/2159-8290.CD-14-0863) [Medline](#)
8. R. S. Herbst, J. C. Soria, M. Kowanetz, G. D. Fine, O. Hamid, M. S. Gordon, J. A. Sosman, D. F. McDermott, J. D. Powderly, S. N. Gettinger, H. E. Kohrt, L. Horn, D. P. Lawrence, S. Rost, M. Leabman, Y. Xiao, A. Mokatrin, H. Koeppen, P. S. Hegde, I. Mellman, D. S. Chen, F. S. Hodi, Predictive correlates of response to the anti-PD-L1 antibody MPDL3280A in cancer patients. *Nature* **515**, 563–567 (2014). [doi:10.1038/nature14011](https://doi.org/10.1038/nature14011) [Medline](#)
 9. N. A. Rizvi, M. D. Hellmann, A. Snyder, P. Kvistborg, V. Makarov, J. J. Havel, W. Lee, J. Yuan, P. Wong, T. S. Ho, M. L. Miller, N. Rekhtman, A. L. Moreira, F. Ibrahim, C. Bruggeman, B. Gasmi, R. Zappasodi, Y. Maeda, C. Sander, E. B. Garon, T. Merghoub, J. D. Wolchok, T. N. Schumacher, T. A. Chan, Mutational landscape determines sensitivity to PD-1 blockade in non-small cell lung cancer. *Science* **348**, 124–128 (2015). [doi:10.1126/science.aaa1348](https://doi.org/10.1126/science.aaa1348) [Medline](#)
 10. W. Hugo, J. M. Zaretsky, L. Sun, C. Song, B. H. Moreno, S. Hu-Lieskovan, B. Berent-Maoz, J. Pang, B. Chmielowski, G. Cherry, E. Seja, S. Lomeli, X. Kong, M. C. Kelley, J. A. Sosman, D. B. Johnson, A. Ribas, R. S. Lo, Genomic and transcriptomic features of response to anti-PD-1 therapy in metastatic melanoma. *Cell* **168**, 542 (2017). [doi:10.1016/j.cell.2017.01.010](https://doi.org/10.1016/j.cell.2017.01.010) [Medline](#)
 11. N. H. Segal, D. W. Parsons, K. S. Peggs, V. Velculescu, K. W. Kinzler, B. Vogelstein, J. P. Allison, Epitope landscape in breast and colorectal cancer. *Cancer Res.* **68**, 889–892 (2008). [doi:10.1158/0008-5472.CAN-07-3095](https://doi.org/10.1158/0008-5472.CAN-07-3095) [Medline](#)
 12. M. M. Gubin, X. Zhang, H. Schuster, E. Caron, J. P. Ward, T. Noguchi, Y. Ivanova, J. Hundal, C. D. Arthur, W. J. Krebber, G. E. Mulder, M. Toebes, M. D. Vesely, S. S. Lam, A. J. Korman, J. P. Allison, G. J. Freeman, A. H. Sharpe, E. L. Pearce, T. N. Schumacher, R. Aebersold, H. G. Rammensee, C. J. Melief, E. R. Mardis, W. E. Gillanders, M. N. Artyomov, R. D. Schreiber, Checkpoint blockade cancer immunotherapy targets tumour-specific mutant antigens. *Nature* **515**, 577–581 (2014). [doi:10.1038/nature13988](https://doi.org/10.1038/nature13988) [Medline](#)
 13. T. N. Schumacher, R. D. Schreiber, Neoantigens in cancer immunotherapy. *Science* **348**, 69–74 (2015). [doi:10.1126/science.aaa4971](https://doi.org/10.1126/science.aaa4971) [Medline](#)
 14. J. P. Ward, M. M. Gubin, R. D. Schreiber, The role of neoantigens in naturally occurring and therapeutically induced immune responses to cancer. *Adv. Immunol.* **130**, 25–74 (2016). [doi:10.1016/bs.ai.2016.01.001](https://doi.org/10.1016/bs.ai.2016.01.001) [Medline](#)
 15. C. Lengauer, K. W. Kinzler, B. Vogelstein, Genetic instabilities in human cancers. *Nature* **396**, 643–649 (1998). [doi:10.1038/25292](https://doi.org/10.1038/25292) [Medline](#)

16. H. Kim, J. Jen, B. Vogelstein, S. R. Hamilton, Clinical and pathological characteristics of sporadic colorectal carcinomas with DNA replication errors in microsatellite sequences. *Am. J. Pathol.* **145**, 148–156 (1994). [Medline](#)
17. T. C. Smyrk, P. Watson, K. Kaul, H. T. Lynch, Tumor-infiltrating lymphocytes are a marker for microsatellite instability in colorectal carcinoma. *Cancer* **91**, 2417–2422 (2001). [doi:10.1002/1097-0142\(20010615\)91:12<2417:AID-CNCR1276>3.0.CO;2-U](https://doi.org/10.1002/1097-0142(20010615)91:12<2417:AID-CNCR1276>3.0.CO;2-U) [Medline](#)
18. R. Dolcetti, A. Viel, C. Doglioni, A. Russo, M. Guidoboni, E. Capozzi, N. Vecchiato, E. Macrì, M. Fornasari, M. Boiocchi, High prevalence of activated intraepithelial cytotoxic T lymphocytes and increased neoplastic cell apoptosis in colorectal carcinomas with microsatellite instability. *Am. J. Pathol.* **154**, 1805–1813 (1999). [doi:10.1016/S0002-9440\(10\)65436-3](https://doi.org/10.1016/S0002-9440(10)65436-3) [Medline](#)
19. D. T. Le, J. N. Uram, H. Wang, B. R. Bartlett, H. Kemberling, A. D. Eyring, A. D. Skora, B. S. Lubner, N. S. Azad, D. Laheru, B. Biedrzycki, R. C. Donehower, A. Zaheer, G. A. Fisher, T. S. Crocenzi, J. J. Lee, S. M. Duffy, R. M. Goldberg, A. de la Chapelle, M. Koshiji, F. Bhajee, T. Huebner, R. H. Hruban, L. D. Wood, N. Cuka, D. M. Pardoll, N. Papadopoulos, K. W. Kinzler, S. Zhou, T. C. Cornish, J. M. Taube, R. A. Anders, J. R. Eshleman, B. Vogelstein, L. A. Diaz Jr., PD-1 blockade in tumors with mismatch-repair deficiency. *N. Engl. J. Med.* **372**, 2509–2520 (2015). [doi:10.1056/NEJMoa1500596](https://doi.org/10.1056/NEJMoa1500596) [Medline](#)
20. M. Overman, S. Lonardi, F. Leone, R. S. McDermott, M. A. Morse, K. Y. M. Wong, B. Neyns, J. L. Leach, P. Garcia Alfonso, J. J. Lee, A. Hill, H.-J. Lenz, J. Desai, R. A. Moss, Z. A. Cao, J.-M. Ledezne, H. Tang, S. Kopetz, T. Andre, Nivolumab in patients with DNA mismatch repair deficient/microsatellite instability high metastatic colorectal cancer: Update from CheckMate 142. *J. Clin. Oncol.* **35** (suppl.), 519 (2017). [doi:10.1200/JCO.2017.35.4_suppl.519](https://doi.org/10.1200/JCO.2017.35.4_suppl.519)
21. A. Grothey, E. Van Cutsem, A. Sobrero, S. Siena, A. Falcone, M. Ychou, Y. Humblet, O. Bouché, L. Mineur, C. Barone, A. Adenis, J. Tabernero, T. Yoshino, H. J. Lenz, R. M. Goldberg, D. J. Sargent, F. Cihon, L. Cupit, A. Wagner, D. Laurent, Regorafenib monotherapy for previously treated metastatic colorectal cancer (CORRECT): An international, multicentre, randomised, placebo-controlled, phase 3 trial. *Lancet* **381**, 303–312 (2013). [doi:10.1016/S0140-6736\(12\)61900-X](https://doi.org/10.1016/S0140-6736(12)61900-X) [Medline](#)
22. J. M. Zaretsky, A. Garcia-Diaz, D. S. Shin, H. Escuin-Ordinas, W. Hugo, S. Hu-Lieskovan, D. Y. Torrejon, G. Abril-Rodriguez, S. Sandoval, L. Barthly, J. Saco, B. Homet Moreno, R. Mezzadra, B. Chmielowski, K. Ruchalski, I. P. Shintaku, P. J. Sanchez, C. Puig-Saus, G. Cherry, E. Seja, X. Kong, J. Pang, B. Berent-Maoz, B. Comin-Anduix, T. G. Graeber, P. C. Tumeh, T. N. Schumacher, R. S. Lo, A. Ribas, Mutations associated with acquired resistance to PD-1 blockade in melanoma. *N. Engl. J. Med.* **375**, 819–829 (2016). [doi:10.1056/NEJMoa1604958](https://doi.org/10.1056/NEJMoa1604958) [Medline](#)

23. R. J. Hause, C. C. Pritchard, J. Shendure, S. J. Salipante, Classification and characterization of microsatellite instability across 18 cancer types. *Nat. Med.* **22**, 1342–1350 (2016). [doi:10.1038/nm.4191](https://doi.org/10.1038/nm.4191) [Medline](#)
24. V. Anagnostou, K. N. Smith, P. M. Forde, N. Niknafs, R. Bhattacharya, J. White, T. Zhang, V. Adleff, J. Phallen, N. Wali, C. Hruban, V. B. Guthrie, K. Rodgers, J. Naidoo, H. Kang, W. Sharfman, C. Georgiades, F. Verde, P. Illei, Q. K. Li, E. Gabrielson, M. V. Brock, C. A. Zahnow, S. B. Baylin, R. B. Scharpf, J. R. Brahmer, R. Karchin, D. M. Pardoll, V. E. Velculescu, Evolution of neoantigen landscape during immune checkpoint blockade in non-small cell lung cancer. *Cancer Discov.* **7**, 264–276 (2017). [doi:10.1158/2159-8290.CD-16-0828](https://doi.org/10.1158/2159-8290.CD-16-0828) [Medline](#)
25. C. S. Carlson, R. O. Emerson, A. M. Sherwood, C. Desmarais, M. W. Chung, J. M. Parsons, M. S. Steen, M. A. LaMadrid-Herrmannsfeldt, D. W. Williamson, R. J. Livingston, D. Wu, B. L. Wood, M. J. Rieder, H. Robins, Using synthetic templates to design an unbiased multiplex PCR assay. *Nat. Commun.* **4**, 2680 (2013). [doi:10.1038/ncomms3680](https://doi.org/10.1038/ncomms3680) [Medline](#)
26. H. S. Robins, P. V. Campregher, S. K. Srivastava, A. Wachter, C. J. Turtle, O. Kahsai, S. R. Riddell, E. H. Warren, C. S. Carlson, Comprehensive assessment of T-cell receptor β -chain diversity in $\alpha\beta$ T cells. *Blood* **114**, 4099–4107 (2009). [doi:10.1182/blood-2009-04-217604](https://doi.org/10.1182/blood-2009-04-217604) [Medline](#)
27. J. W. Bacher, L. A. Flanagan, R. L. Smalley, N. A. Nassif, L. J. Burgart, R. B. Halberg, W. M. Megid, S. N. Thibodeau, Development of a fluorescent multiplex assay for detection of MSI-high tumors. *Dis. Markers* **20**, 237–250 (2004). [doi:10.1155/2004/136734](https://doi.org/10.1155/2004/136734) [Medline](#)
28. K. M. Murphy, S. Zhang, T. Geiger, M. J. Hafez, J. Bacher, K. D. Berg, J. R. Eshleman, Comparison of the microsatellite instability analysis system and the Bethesda panel for the determination of microsatellite instability in colorectal cancers. *J. Mol. Diagn.* **8**, 305–311 (2006). [doi:10.2353/jmoldx.2006.050092](https://doi.org/10.2353/jmoldx.2006.050092) [Medline](#)
29. J. D. Wolchok, A. Hoos, S. O’Day, J. S. Weber, O. Hamid, C. Lebbé, M. Maio, M. Binder, O. Bohnsack, G. Nichol, R. Humphrey, F. S. Hodi, Guidelines for the evaluation of immune therapy activity in solid tumors: Immune-related response criteria. *Clin. Cancer Res.* **15**, 7412–7420 (2009). [doi:10.1158/1078-0432.CCR-09-1624](https://doi.org/10.1158/1078-0432.CCR-09-1624) [Medline](#)
30. N. J. Llosa, M. Cruise, A. Tam, E. C. Wicks, E. M. Hechenbleikner, J. M. Taube, R. L. Blosser, H. Fan, H. Wang, B. S. Lubner, M. Zhang, N. Papadopoulos, K. W. Kinzler, B. Vogelstein, C. L. Sears, R. A. Anders, D. M. Pardoll, F. Housseau, The vigorous immune microenvironment of microsatellite instable colon cancer is balanced by multiple counter-inhibitory checkpoints. *Cancer Discov.* **5**, 43–51 (2015). [doi:10.1158/2159-8290.CD-14-0863](https://doi.org/10.1158/2159-8290.CD-14-0863) [Medline](#)

31. J. M. Taube, R. A. Anders, G. D. Young, H. Xu, R. Sharma, T. L. McMiller, S. Chen, A. P. Klein, D. M. Pardoll, S. L. Topalian, L. Chen, Colocalization of inflammatory response with B7-H1 expression in human melanocytic lesions supports an adaptive resistance mechanism of immune escape. *Sci. Transl. Med.* **4**, 127ra37 (2012).
[doi:10.1126/scitranslmed.3003689](https://doi.org/10.1126/scitranslmed.3003689) [Medline](#)
32. N. Cuka, H. Hempel, K. Sfanos, A. De Marzo, T. Cornish, PIP: An open source framework for multithreaded image analysis of whole slide images. *Lab. Invest.* **94**, 398A (2014).
33. J. Cupitt, K. Martinez, in *Electronic Imaging: Science & Technology* (International Society for Optics and Photonics, 1996), pp. 19–28.
34. S. Jones, V. Anagnostou, K. Lytle, S. Parpart-Li, M. Nesselbush, D. R. Riley, M. Shukla, B. Chesnick, M. Kadan, E. Papp, K. G. Galens, D. Murphy, T. Zhang, L. Kann, M. Sausen, S. V. Angiuoli, L. A. Diaz Jr., V. E. Velculescu, Personalized genomic analyses for cancer mutation discovery and interpretation. *Sci. Transl. Med.* **7**, 283ra53 (2015).
[doi:10.1126/scitranslmed.aaa7161](https://doi.org/10.1126/scitranslmed.aaa7161) [Medline](#)
35. M. Sausen, R. J. Leary, S. Jones, J. Wu, C. P. Reynolds, X. Liu, A. Blackford, G. Parmigiani, L. A. Diaz Jr., N. Papadopoulos, B. Vogelstein, K. W. Kinzler, V. E. Velculescu, M. D. Hogarty, Integrated genomic analyses identify ARID1A and ARID1B alterations in the childhood cancer neuroblastoma. *Nat. Genet.* **45**, 12–17 (2013). [doi:10.1038/ng.2493](https://doi.org/10.1038/ng.2493)
[Medline](#)
36. S. B. Needleman, C. D. Wunsch, A general method applicable to the search for similarities in the amino acid sequence of two proteins. *J. Mol. Biol.* **48**, 443–453 (1970).
[doi:10.1016/0022-2836\(70\)90057-4](https://doi.org/10.1016/0022-2836(70)90057-4) [Medline](#)